Separation Science and Technology
Publication details, including instructions for authors and subscription information:
http://www.informaworld.com/smpp/title~content=t713708471

Prediction of Charge Density for Desal-HL Nanofiltration Membrane from Simulation and Experiment using Different Ion Radii

A. A. Hussain[a]; M. E. E. Abashar[a]; I. S. Al-Mutaz[a]
[a] Chemical Engineering Department, College of Engineering, King Saud University, Riyadh, Saudi Arabia

To cite this Article Hussain, A. A. , Abashar, M. E. E. and Al-Mutaz, I. S.(2007) 'Prediction of Charge Density for Desal-HL Nanofiltration Membrane from Simulation and Experiment using Different Ion Radii', Separation Science and Technology, 42: 1, 43 — 57
To link to this Article: DOI: 10.1080/01496390600998003
URL: http://dx.doi.org/10.1080/01496390600998003

Separation Science and Technology, 42: 43–57, 2007

ISSN 0149-6395 print/1520-5754 online
DOI: 10.1080/01496390600998003

Prediction of Charge Density for Desal-HL Nanofiltration Membrane from Simulation and Experiment using Different Ion Radii

A. A. Hussain, M. E. E. Abashar, and I. S. Al-Mutaz
Chemical Engineering Department, College of Engineering, King Saud University, Riyadh, Saudi Arabia

Abstract: Solute separation characteristics of commercial nanofiltration (NF) membrane Desal-HL were investigated. Donnan steric pore model (DSPM) was applied to the experimental data to study the charge density at the surface of the membrane for various solute radii namely Stokes-Einstein, Born, and Pauling. Sodium chloride and magnesium chloride were used as simple solutes. The effect of pH was studied for all the solutes. Correlations for the charge density for each radius were proposed. It was found that the charge density changes considerably with the ion radius, and, consequently causes remarkable variations in prediction of ions rejections.

Keywords: Membrane separation, nanofiltration, charge density, DSPM, pH effect, Stokes-Einstein radius, Born radius, Pauling radius

INTRODUCTION

There is an increased interest in focusing the use of nanofiltration (NF) membrane technology for separation processes in the chemical and biological industry because it overcomes several operational problems associated with conventional techniques. The NF membrane lies between ultrafiltration (UF) and reverse osmosis (RO) with former being porous in structure and the latter being non porous. NF membranes take into account the sieving

Received 20 May 2006, Accepted 21 August 2006
Address correspondence to A. A. Hussain, Chemical Engineering Department, College of Engineering, King Saud University, P.O. Box 800, Riyadh 11421, Saudi Arabia. E-mail: altafchem@yahoo.com.au

and electrical effects of UF and solution diffusion of RO, which allows it to separate charged organic solutes and inorganic solutes.

The application of NF technology today includes pretreatment in sea water desalination (1), disinfection by removal of virus, removal of pesticides and other micro pollutants, arsenic removal, recovery of high value organometallic catalysts from reaction mixtures allowing the catalyst to be reused (2). Pharmaceutical applications include isolation of industrially important antiviral drug precursor N-acetyl-D-neuraminic acid (3), clindamycin from fermentation waste water (4), sodium cefuroxime from cephalosporin-C (5), and cephalexin (6).

In order to fully realize the application potential of NF and to properly predict the membrane performance, it is important to have a mathematical transport model. The ionic transport and the selectivity of NF membranes mainly depend on two effects: charge repulsion and steric/hydrodynamic effects. The first effect is caused by the charged nature of the membrane and electrolytes. The second effect is caused by the relative size of the ions to the membrane pores. Additional phenomena can affect membrane performance namely ion-membrane affinity, specific adsorption, reduced dielectric permittivity, and hydration. Models for NF are usually based either on a mechanism-independent approach, such as irreversible thermodynamics or structural mechanism dependence (7). The models based on irreversible thermodynamics treat the membrane as a black box ignoring the structure of the membrane or any transport mechanism. Mechanistic models assume a membrane structure and the model equations account for the effects of physical and chemical characteristics of both the membrane and electrolyte solution. Most mechanistic models fall in two categories: those based on the space-charge (SC) model (8) and Teorrell-Meyer-Sievers (TMS) model (9). The SC model is mathematically complicated and computationally expensive when compared with the TMS model. Donnan steric pore model (DSPM) is an extension of TMS model with additional modifications.

Original DSPM contains three fitting parameters namely, pore radius, membrane thickness and charge density. Bowen and co-workers (10) by including the partial molar volume of solute and pore viscosity resulted that NF membrane performance can be predicted by two fitting parameters namely radius of pore and charge density. The proposed DSPM was independent of membrane thickness and depends only on two parameters namely radius of pore and charge density. The DSPM succeeded to predict the membrane performance in a limited range of operating conditions (10). However, the semi-empirical DSPM and other existing models suffer from many problems such as:

(a) the large predicted effective charge density,
(b) membrane characterization is performed through a complex fitting procedure,
(c) the models fail to predict successfully the rejection of many ions.

The DSPM assumes the Donnan equilibrium as the only electrostatic phenomenon involved in the ion partitioning. It is a matter of fact that the Donnan equilibrium is not sufficient to explain the high rejection values of the model compared to experimental values for many ions. A physical assessment of the separation phenomena take place in many systems indicates that many factors are being taken into account implicitly in the DSPM, which result in a poor quality of agreement with experimental data in many cases. To this end, general good predictive models till now do not exist for prediction of simple single salts rejections such as sodium chloride, magnesium chloride etc.

Currently, there is no unified model, describing NF membranes in all their variety. There are also a limited number of publications on the experimental determination of ion sizes. According to our knowledge, there is no existing study that considers the effect of variations of ion sizes on assessing the membrane parameters.

In the present study, the DSPM is used to estimate the charge density at the surface of Desal-HL (GE Osmonic, USA) NF membrane. Special attention is paid to the role of ion sizes on the performance of the membrane. Various ion radii (Stokes-Einstein, Born's effective, Pauling) are considered. Model calculation and predictions are compared with experimental data. The effect of the pH on the performance of the membrane is also considered. Simple systems are chosen for study, sodium and magnesium chlorides.

THEORETICAL MODELING

One-dimensional Donnan steric pore model is considered for transport of electrolytes through NF membranes. A schematic diagram of the coordinate system used is shown in Fig. 1.

The assumptions and detailed derivation of the model are given by Bowen et al (10). The governing equations and their boundary conditions are given as

$$\frac{dc_i}{dx} = \left[\left[K_{ic} - \left(\frac{8\eta}{RTr_p^2}\right)D_{ip}V_i\right]c_i - C_i(\delta^+)\right]\frac{u}{D_{ip}} - \frac{F}{RT}z_i c_i \frac{d\psi}{dx} \quad (1)$$

$$\frac{d\psi}{dx} = \frac{\sum_{i=1}^{n}[[K_{ic} - (8\eta/RTr_p^2)\ D_{ip}V]c_i - C_i(\delta^+)]z_i u/D_{ip}}{F/RT\sum_{i=1}^{n} z_i^2 c_i} \quad (2)$$

The ionic partition coefficient of ion i accounts for different physicochemical interactions between the ions in solution and between the ions in

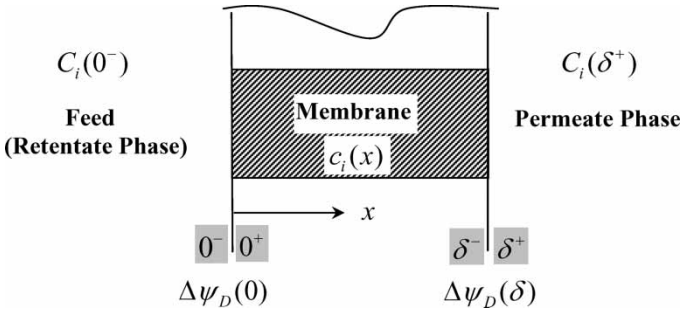

Figure 1. Coordinate system for the DSPM.

the pores and the membrane matrix and may be written as:

$$k_i = (\text{steric}) \times [\text{electrostatic (Donnan)}] \times [\text{solvation (Born)}] \times (\text{dielectric}) \times \ldots \tag{3}$$

Equations 1 and 2 form a boundary value problem with the following boundary conditions:

$$at\ x = 0$$

$$k_i|_0 = \frac{c_i(x)|_{x=0^+}}{C_i(0^-)} = \phi_i \exp\left(-\frac{Fz_i}{RT}\Delta\psi_D(0)\right) \tag{4}$$

$$at\ x = \delta$$

$$k_i|_\delta = \frac{c_i(x)|_{x=\delta^-}}{C_i(\delta^+)} = \phi_i \exp\left(-\frac{Fz_i}{RT}\Delta\psi_D(\delta)\right) \tag{5}$$

The pore wise rejection of solute i is given by

$$R_i = 1 - \frac{C_i(\delta^+)}{C_i(0^-)} \tag{6}$$

MATERIALS AND METHODS

Desal-HL (GE Osmonic, USA) NF membrane was chosen for study. They are flat sheet type and thin film composite membrane made by interfacial polymerization of polysulfone base with recommended pH range of 3–9. The thin active layer is proprietary polyamides. Three types of inorganic electrolytes namely sodium chloride, sodium sulphate, and magnesium chloride were employed in the permeation experiment. The concentration and the pH value of inorganic electrolyte solution were measured with an electrical conductivity meter (Oakton Inc.) and a pH meter (Oakton Inc.). The experimental rig was procured from GE Osmonic namely E2 series and the total area of

membrane was 2.4 m^2. The schematic diagram of the experimental rig is shown in Fig. 2. The permeation experiments were carried out under the applied condition of 0.2–1.1 MPa. The retentate and permeate are recycled back to the feed tank in order to hold the concentration of the feed solution constant. Glucose was used as neutral solute to estimate the radius of pore. The concentration of glucose was determined by phenol-sulphuric acid method (11). The concentration of sodium chloride, sodium sulphate, and magnesium chloride was kept at 10 mol/m^3. The viscosity of the solution was considered to be same as that of pure water. All the solutes were nanofiltered and their pH was adjusted from 3 to 9 using sodium hydroxide and sulphuric acid.

Description of Different Solute Radii

In this study we considered three ion radii namely Stokes-Einstein, Born's effective and Pauling. The Stokes-Einstein radius is derived from Stokes-Einstein relation (12):

$$r_S = \frac{kT}{6\pi\eta_o D_{i\infty}} \tag{7}$$

The Born's effective radius is derived from Born theory. Fig. 3 illustrates the structure of solutes, which consists of a bare ion radius interacting with the solvent. As it can be seen a cation is surrounded by water molecules with

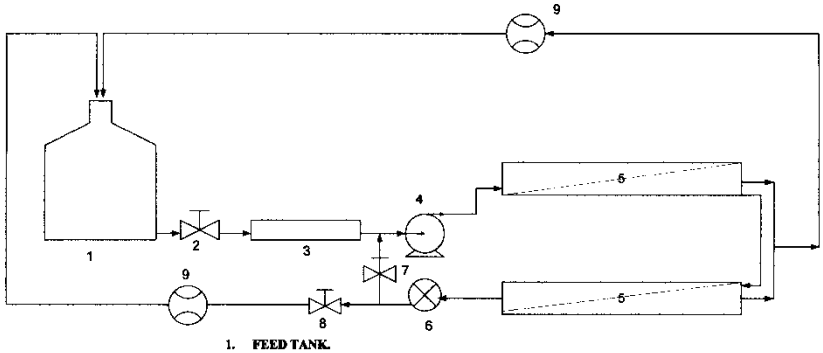

Figure 2. Schematic diagram of experimental test rig.

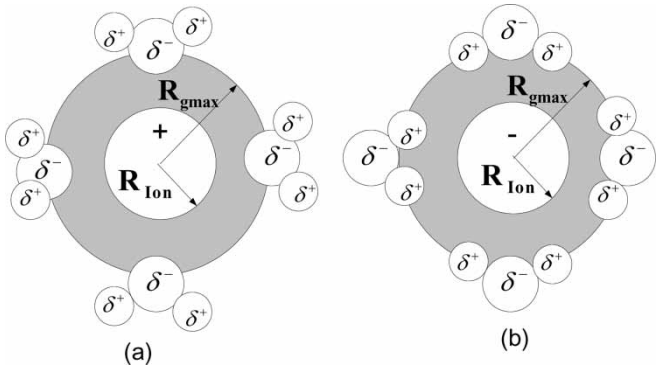

Figure 3. A schematic diagram of the orientation of water dipoles around (a) cations and (b) anions (13).

oxygen atoms approaching them, while an anion is surrounded by water molecules with hydrogen atoms approaching them. R_{ion} is the ionic radius and is purely a property of the ion. R_{gmax} is defined as the position of the first peak in the ion-solvent radial distribution function; it depends on both the ion and the molecular nature of the solvent. The Born model has been successfully used to treat the solvation free energy of an ion. However, the use of ionic radius (R_{ion}) overestimates the magnitude of the solvation energy. Babu and Lim (13) have shown by using molecular dynamics simulation of ions of varying charges, that the Born's effective radius is given by:

$$r_B = (R_{ion} + R_{g\,\max})/2.0 \tag{8}$$

Pauling radius is defined as the bare ion crystal radius. Recent rejection measurements for ion mixtures using artificial nanofilters have shown that Pauling radius is the best choice (12). The physical properties of all ions and solutes used in the study are shown in Table 1.

Table 1. Parameters used in the simulation (12–17)

Solute	$D_{i\infty}\ 10^{-9}\ m^2\ s^{-1}$	$V_i\ cm^3\ mol^{-1}$	r_S nm	r_B nm	r_{Pa} nm
Na^+	1.33	−1.20	0.184	0.169	0.095
Cl^-	2.03	17.82	0.121	0.202	0.181
Mg^{2+}	0.72	−21.57	0.341	0.142	0.065
SO_4^{2-}	1.06	14.18	0.231	0.258	0.290

COMPUTATIONAL PROCEDURE

Equations 1 and 2 are solved by shooting method based on Runge-Kutta Gear method and Newton-Raphson technique using FORTRAN subroutines namely DGEAR and ZSPOW. Double precision was used in all simulation.

RESULTS AND DISCUSSIONS

Determination of Membrane Permeability and Pore Radius

The model was fitted with the experimental data using the least square analysis to estimate the membrane permeability and the pore radius. The permeability and radius of pore were 22.87×10^{-6} m/s · Pa and 0.48 nm respectively. The radius of pore was determined using uncharged solute rejection of glucose. The electromigration term in equation 1 was cancelled as neutral solutes do not carry charge. It results in an analytical expression relating rejection with pressure drop. The radius of pore is the fitting parameter to the experimental rejection. Least square analysis was employed.

Effect of pH

Figure 4 summarizes the rejection behavior of sodium chloride, sodium sulphate, and magnesium chloride with pH. Sodium chloride rejection was low with respect to all the solutes and minimum rejection was observed at isoelectric point where the membrane is uncharged at pH 5.5. The isoelectric point corresponds to the value of pH for which the electric charge of the fixed cations globally neutralizes that of the anion. The positive charge of the membrane grows when the pH decreases and the Na^+ ions are more and more rejected by the A-NH_3+ groups of the membrane. As the cation and anion cannot act independently, Cl^- is also rejected to maintain the electroneutrality. The charge effect is thus added to the steric exclusion phenomenon and the retention increases. When the pH is increased above the isoelectric point will result in increase of negative charge at the surface of the membrane, due to that more Cl^- will get rejected. The rejection behavior of sodium sulphate is completely different from sodium chloride as shown in Figure 4. Rejection increases sharply and remains constant above the isoelectric point. At lower pH, sodium sulphate exhibited lower rejection and possible explanation is due to the expansion of polymeric matrix. Above isoelectric, the rejection remains constant and results in compression of pore due to the hydroxyl ion present in the water. The rejection profile of magnesium chloride shows a maximum rejection at isoelectric. At lower and higher pH, the expansion of pore takes place resulted in lower rejection and at isoelectric point, the rejection was high due to the compression of

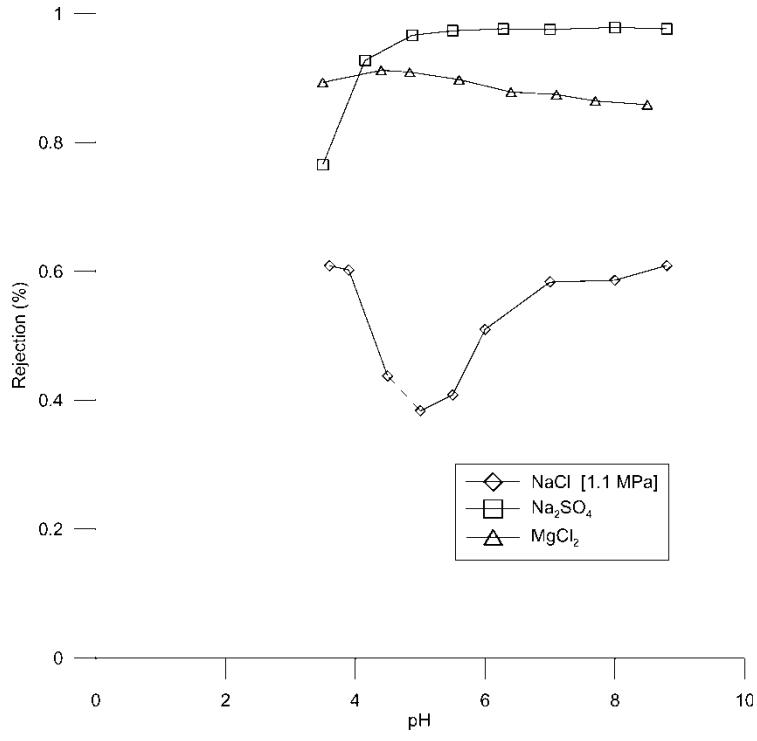

Figure 4. Effect of solute type on the separation dependency on pH for various solutes at 0.01 M concentration.

polymer matrix results in decrease in pore radius. One of the interesting aspects is that when the membrane was positively charged, the rejection of magnesium chloride was higher than the sodium sulphate which was also observed by certain researchers (18, 19).

The DSPM model was fitted with experimental data using various radii to get the charge density across the surface of the membrane. For sodium chloride, the charge densities for positively charged membrane (on left side of the isoelectric point) and negatively charged membrane (on right side of the isoelectric point) for Stokes radius are shown in Figs 5 and 6 respectively. A similar procedure is done for the other radii.

The corresponding charge densities for positively and negatively charged membrane are shown in Tables 2 and 3 respectively.

Two sets of correlations are obtained for each region. For positive charge density the following correlations were obtained:

$$\begin{array}{ll} \text{Stokes Einstein radius} & \chi_d = -47.91pH + 291.34 \\ \text{Born's effective radius} & \chi_d = -34.06pH + 210.49 \\ \text{Pauling radius} & \chi_d = -108.68pH + 661.11 \end{array} \quad (9)$$

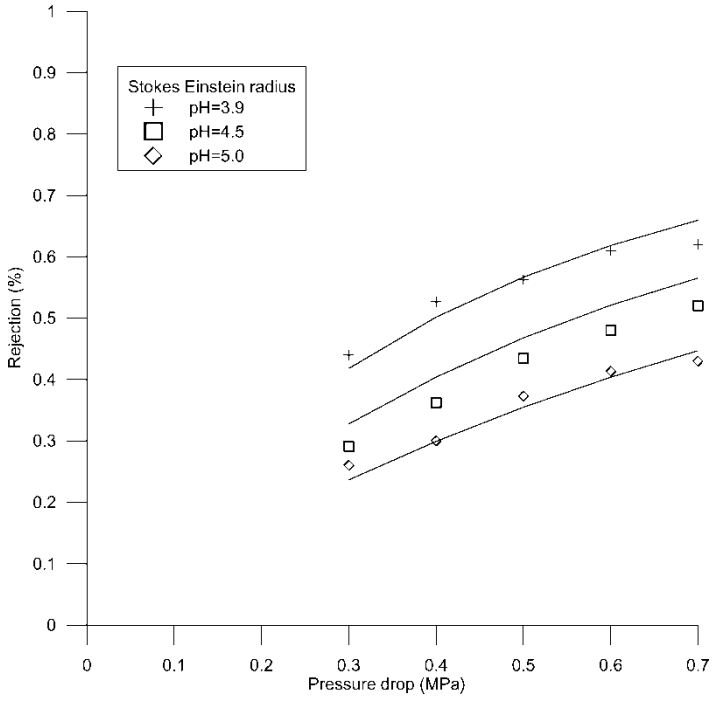

Figure 5. Experimental and theoretical rejection of sodium chloride of 0.01 M concentration for various pH values for Stokes Einstein radius. (positive charge density).

And for negative charge density the following correlations were obtained

$$\begin{array}{ll} \text{Stokes Einstein radius} & \chi_d = -38.44pH + 69.89 \\ \text{Born's effective radius} & \chi_d = -13.36pH + 25.55 \\ \text{Pauling radius} & \chi_d = -30.14pH + 67.34 \end{array} \quad (10)$$

Figure 7 (a) shows that the difference between the experimental and the predicted values of the positive charge density for all radii is less than $\pm 16\%$. The difference between the experimental and the predicted values of the negative charge density for all radii is less than $\pm 5\%$ as shown in Fig. 7(b).

Figure 8 shows the experimental and theoretical rejection based on Stokes Einstein for magnesium chloride for various pH. The membrane behaves as a positive charged surface. The fitted charge density is shown in Table 4. Born's effective and Pauling radii were also treated similarly.

The following correlations are obtained:

$$\begin{array}{ll} \text{Stokes Einstein radius} & \chi_d = 4.03pH - 4.94 \\ \text{Born's effective radius} & \chi_d = 19.47pH - 21.11 \\ \text{Pauling radius} & \chi_d = 32.33pH - 25.53 \end{array} \quad (11)$$

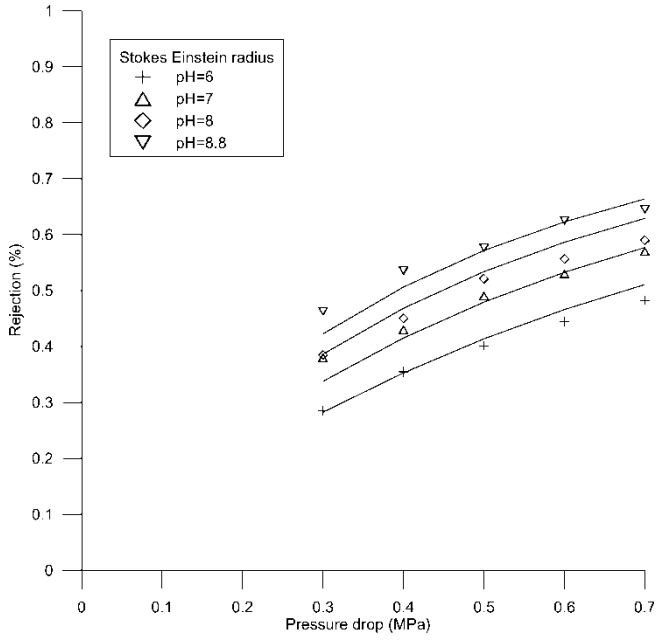

Figure 6. Experimental and theoretical rejection of sodium chloride of 0.01 M concentration for various pH values for Stokes Einstein radius. (negative charge density).

Table 2. Effect of pH on charge density for sodium chloride with various radii (positive charge)

	Stokes Einstein radius	Born's effective radius	Pauling radius
pH	χ_d (mol m^{-3})	χ_d (mol m^{-3})	χ_d (mol m^{-3})
3.9	108.0	80.0	245.0
4.5	68.0	52.0	155.0
5.0	56.0	43.0	127.0

Table 3. Effect of pH on charge density for sodium chloride with various radii (negative charge)

	Stokes Einstein radius	Born's effective radius	Pauling radius
pH	χ_d (mol m^{-3})	χ_d (mol m^{-3})	χ_d (mol m^{-3})
6.0	−156.0	−53.0	−111.0
7.0	−210.0	−72.0	−152.0
8.0	−230.0	−78.0	−164.0
8.8	−272.0	−93.0	−202.0

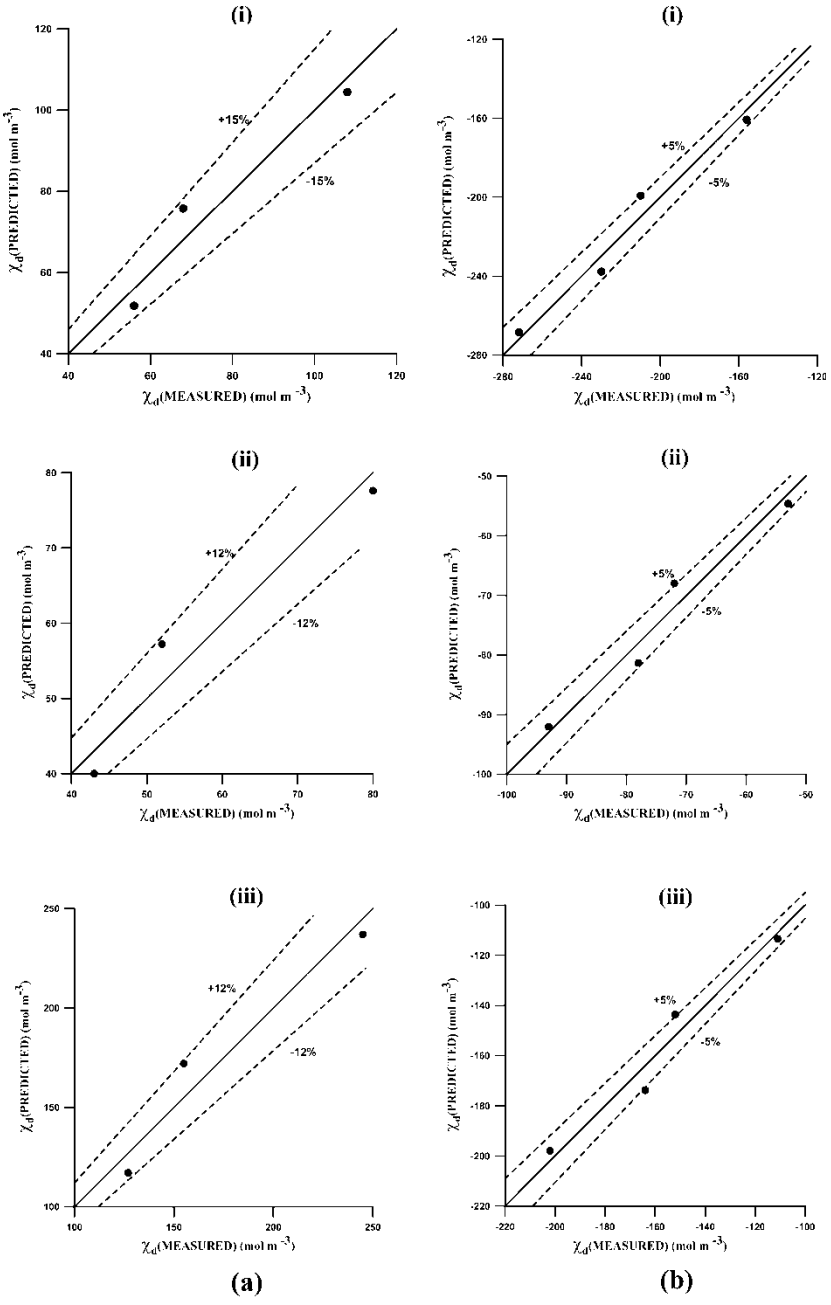

Figure 7. Parity plot for the charge density using sodium chloride with various radii ((i) for Stokes, (ii) for Born, (iii) for Pauling): (a) positive charge; (b) negative charge.

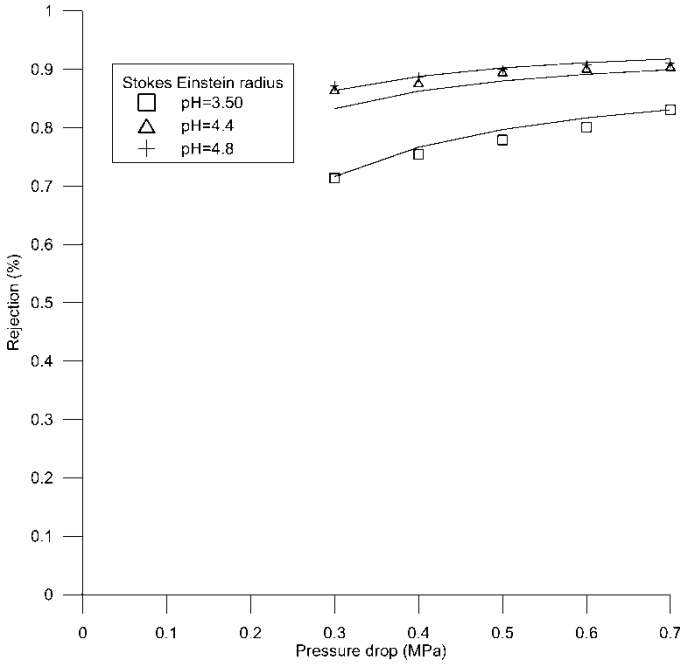

Figure 8. Experimental and theoretical rejection of magnesium chloride of 0.01 M concentration for various pH values for Stokes Einstein radius.

As can be seen from Fig. 9 that the difference between the experimental and the predicted values of charge density for all radii is less than $\pm$ 10%.

CONCLUSIONS

The results reported showed that there was a marked difference in the predicted charge density at the surface of the membrane when different ion radii are used. This indicates that for better understanding and prediction of

Table 4. Effect of pH on charge density for magnesium chloride with various radii (positive charge)

	Stokes Einstein radius	Born's effective radius	Pauling radius
pH	χ_d (mol m^{-3})	χ_d (mol m^{-3})	χ_d (mol m^{-3})
3.5	8.9	46.0	86.0
4.4	13.7	68.0	122.0
4.8	13.8	70.0	126.0

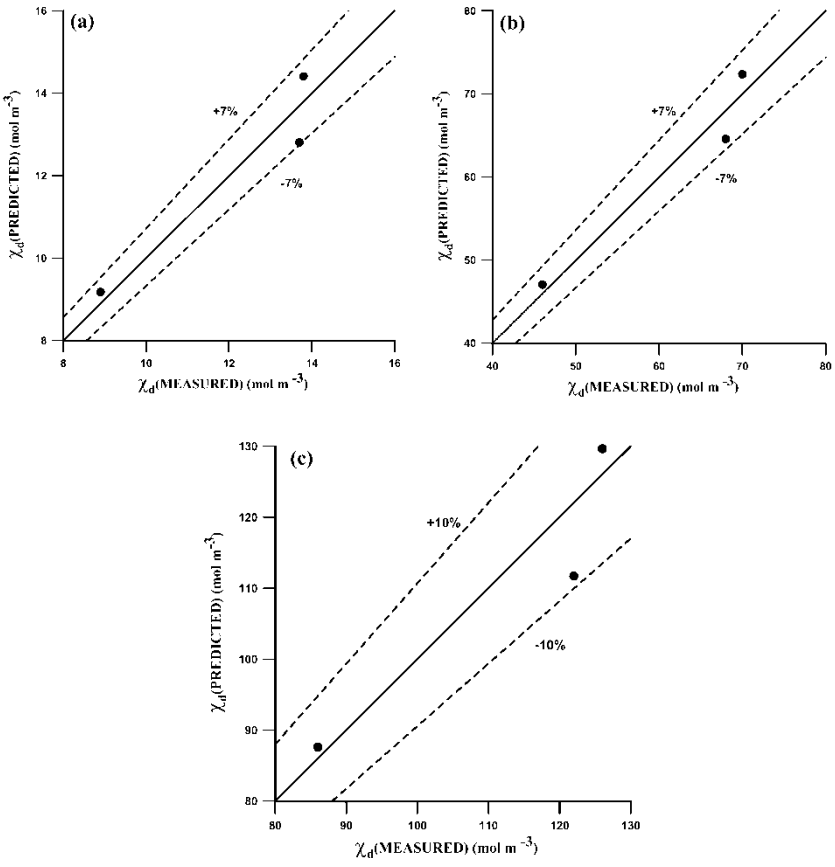

Figure 9. Parity plot for the charge density using magnesium chloride with various radii: (a) Stokes radius, (b) Born radius, (c) Pauling radius.

membrane performance is to determine the ion size accurately, which may affect significantly the surface electrical properties of the membrane. The correlations developed in this article provide good estimation of the charge density. It was found that the pH has great influence on the charge density. The present work contributes to the relatively scarce data in the literature on this kind of investigation.

SYMBOLS

0^-	feed/membrane interface, feed side
0^+	feed/membrane interface, membrane side
$C_i(0^-)$	solute feed solution concentration, (mol m^{-3})
$C_i(\delta^+)$	solute permeate solution concentration, (mol m^{-3})

$c_i(x)$	concentration of ion i within pore, (mol m^{-3})
D_{ip}	pore diffusion coefficient of ion i, (m^2s^{-1})
$D_{i\infty}$	ion bulk diffusion coefficient, (m^2s^{-1})
F	Faradays constant, (96487 $Cmol^{-1}$)
j_i	flux of ion i, (mol m^{-2} s^{-1})
k	Boltzmann constant, (1.38066×10^{-23} JK^{-1})
k_i	ionic partition coefficient of ion i, dimensionless (−)
$K_{i,c}$	hindrance factor for convection of ion i, dimensionless(−)
r_B	Born radius of ion i, (m)
r_{Pa}	Pauling radius of ion i, (m)
r_p	radius of pore, (m)
r_S	Stokes-Einstein radius of ion i, (m)
R_i	overall rejection of solute i, calculated through equation (6), dimensionless (−)
R	universal gas constant, (8.314 $Jmol^{-1}K^{-1}$)
T	absolute temperature, (K)
u	solvent velocity, (ms^{-1})
V_i	partial molar volume of ion i, (m^3mol^{-1})
x	axial position within the pore, (m)
z_i	valence of ion i, dimensionless (−)

Greek

δ	membrane thickness, m
$\Delta\psi_D(0)$	Donnan Potential at the feed membrane interface, (V)
$\Delta\psi_D(\delta)$	Donnan Potential at the permeate membrane interface, (V)
η	solvent viscosity within pores, (N s m^{-2})
η_0	bulk solvent viscosity, (N s m^{-2})
ϕ_i	steric partition coefficient of ion i, dimensionless (−)
χ_d	effective charge density, (mol m^{-3})
ψ	potential within the pore, (V)

REFERENCES

1. Hassan, A., Al-Sofi, M.A.K., Al-Amoudi, A., Jamaluddin, A., Farooque, A., Rowaili, A., Dalvi, A., Kither, N., Mustafa, G., and Al-Tisan, I. (1998) A new approach to thermal seawater desalination processes using nanofiltration membranes (part I). *Desalination*, 118: 35.
2. Van der Bruggen, B. and Vandecasteele, C. (2003) Removal of pollutants from surface water and ground water by nanofiltration: overview of possible applications in the drinking water industry. *Environmental Pollution*, 122: 435.
3. Bowen, W.R., Cassey, B., Jones, P., and Oatley, D.L. (2004) Modeling the performance of membrane nanofiltration-application to an industrially relevant separation. *J. Membrane Sci.*, 242: 211.
4. Zhu, A., Zhu, W., Wu, Z., and Jing, Y. (2003) Recovery of clindamycin from fermentation wastewater with nanofiltration membranes. *Water Research*, 37: 3718.

5. Oatley, D.L., Cassey, B., Jones, P., and Bowen, W.R. (2005) Modeling the performance of membrane nanofiltration- recovery of a high value product from a process waste stream. *Chem. Eng. Sci.*, 60: 1953.
6. Wang, K.Y., Xiao, Y., and Chung, T.S. (2006) Chemically modified polybenzimidazole nanofiltration membrane for the separation of electrolytes and ceplalexin. *Chem. Eng. Sci.*, 61: 5507.
7. Spiegler, K. and Kedem, O. (1966) Thermodynamics of hyperfiltration (reverse osmosis). Criteria for efficient membranes. *Desalination*, 1: 311.
8. Gross, R. and Osterele, J. (1961) Membrane transport characteristics of ultrafine capillaries. *J. Chem. Phys.*, 49: 228.
9. Wang, X., Tsuru, T., Nakao, S., and Kimura, S. (1995) Electrolyte transport through nanofiltration membranes by the space charge model and comparison with Teorell-Meyer-Sievers model. *J. Membrane Sci.*, 103: 117.
10. Bowen, W.R. and Welfoot, J.S. (2002) Modeling the performance of membrane nanofiltration- critical assessment and model development. *Chem. Eng. Sci.*, 57: 1121.
11. Dubois, M., Gilles, K.A., Hamilton, K., Rebers, P.A., and Smith, F. (1956) Colorimetric method for determination of sugars and related substances. *Anal. Chem.*, 28: 350.
12. Lefebvre, X., Palmeri, J., and David, P. (2004) Nanofiltration theory: an analytic approach for single salts. *J. Phys. Chem. B*, 108: 16811.
13. Babu, C.S. and Lim, C. (1999) A new interpretation of the effective born radius from simulation and experiment. *Chem. Phys. Lett.*, 310: 225.
14. Atkins, P. and Paula, J.D. (1999) *Atkins Physical Chemistry*, 7th ed.; Oxford University Press: Oxford, U.K.
15. Zilberbrand, M. (1997) A nonelectrical mechanism of ion exchange in thin water films in finely dispersed media. *J. of Colloid and Interface Sci.*, 192: 471.
16. Huheey, J. (1983) *Inorganic Chemistry: Principles of Structure and Reactivity*, 3rd ed.; Harper International SI Edition: New York.
17. Kiyosawa, K. (1991) Volumetric properties of polyols (ethylene glycol, glycerol, meso-erthritol, xylitol and mannitol) in relation to their membrane permeability: group estimation and estimation of the maximum radius of their molecules. *Biochemica et Biophysica Acta-Biomembranes*, 1064: 251.
18. Rios, G.M., Joulie, R., Sarrade, S.J., and Carles, M. (1996) Investigation of ion separation by microporous nanofiltration membranes. *American Institute of Chemical Engineering Journal*, 42: 2521.
19. Xu, Y. and Lebrun, R.E. (1999) Investigation of the solute separation by charged nanofiltration membrane: effect of pH, ionic strength and solute type. *J. Membrane Sci.*, 158: 93.